Available online at www.sciencedirect.com
ScienceDirect
Journal of Sound and Vibration 300 (2007) 831–846
JOURNAL OF SOUND AND VIBRATION
www.elsevier.com/locate/jsvi

Active vibration control of flexible materials found within printing machines

Daniel Greco[a], Philippe Blanc[a], Evelyne Aubry[b], Ivan Vaclavik[a,*]

[a]*University of Applied Sciences, Route de Cheseaux 1, 1401 Yverdon-les-Bains, Switzerland*
[b]*Ecole Supérieure des Sciences Appliquées pour l'Ingénieur de Mulhouse, 12, rue des frères Lumière, 68093 Mulhouse, France*

Received 20 June 2005; received in revised form 4 September 2006; accepted 4 September 2006
Available online 30 October 2006

Abstract

The dynamic characteristics of out-of-plane vibrations of web materials on printing machines are investigated in this study. The solution of the nonlinear equation which describes this motion is computed and compared with the experimental results obtained on a test bed.

The proposed controller is based on the travelling wave theory and on the transfer functions identified from the measurement data. Good experimental results are obtained by implementing the controller on a test bed. The measurements of two printing materials under different excitation frequencies show the effectiveness and robustness of the controller cancelling out vibrations.

1. Introduction

In an economy characterized by eroded margins and profitability, printing companies require from their machines continuously growing productivity and faster speed of moving webs while ensuring excellent printing quality. The vertical or out-of-plane vibrations of paper webs or plastic films caused by unbalanced cylinders or aerodynamic effects can deteriorate the printing quality and even cause web rupture followed by the interruption of production. To avoid these dysfunctions, it is necessary to better understand the dynamics of each element in the printing machines, including the moving webs. In this paper, a web refers to any material of a continuous flexible strip.

The modelling of vertical vibrations of a moving web has been described in several publications, e.g., Refs. [1–3].

The issue of the active compensation of the vibrations of flexible materials is discussed in Refs. [4–9]. In Ref. [5], the control algorithm is obtained through the optimization of the quadratic performance function, in which the locations of the sensors and the actuator are taken into account. Robust control based on the experimentally obtained transfer functions is described in Refs. [8,10]. The transfer function concept with wave cancellation is developed in Refs. [5,7]. The latter principle is used in the present application.

*Corresponding author. Tel.: +41 24 5576 322; fax: +41 24 5576 320.
E-mail address: ivan.vaclavik@heig-vd.ch (I. Vaclavik).

0022-460X/$ - see front matter © 2006 Elsevier Ltd. All rights reserved.
doi:10.1016/j.jsv.2006.09.006

Nomenclature

b	width of the web
c_0	wave propagation or critical speed
D	flexural rigidity
E	elasticity
f	frequency
F	force per unit area exerted by the roller on the flexible web
F_ε	force of large intensity
$G_k(s)$	frequency selective filters transfer function
$G_{ck}(s)$	controller transfer function
h	thickness of the web
$H(x_k, s)$	Laplace transforms of out-of-plane web displacements
K_{pk}	proportional gain
L	length between rollers A and D
m_a	mass of surrounding air per unit length of the web
M_a	mass of the surrounding air
M_p	mass of the flexible material
$R(s)$	controller total transfer function
t	time
T	plane tension
$U(s)$	control force transfer function
V	translatory speed
w	vertical displacement of the web
w_k	initial condition
w_ε	solution of the penalized problem
x	machine direction
x_a	actuator location
x_k	sensor location
y	cross direction
α	coefficient
ε	penalization parameter
φ	function of the parts of rollers in contact with the web
ν	Poisson coefficient
ρ	volume density
τ_k	time constant
υ	dimensionless translatory speed
ζ	damping factor
ω_k	pulsation
Ω	domain

Subscripts

i, j	orders of mode complexities
n	order of natural frequencies

In the case of a two-dimensional model with some boundary conditions and with obstacles, it is not possible to obtain an analytical solution.

The problem is solved numerically in Section 3.1 using the finite difference method.

In Section 3.2, the formulas from publication [1] based on the linear model of a web [11], which takes account of the surrounding airflow are presented.

The measurement results of the vibrations are represented in Section 4 on two and three dimensional maps. The optimal locations of the sensors and of the actuator are also discussed in this section.

The last two sections focus on the synthesis and experimental verification of the active compensation for out-of-plane vibrations of the web with two displacement sensors, two controllers and an actuator.

The efficiency of the proposed control structure is experimentally verified in Section 6 with the web excited by the 1st vibration mode. Control robustness is further tested by modifying the disturbance frequency and the tension applied to the flexible web.

2. Test bed specifications

The experimental setup is shown in Fig. 1. The vertical displacement w(x, y, t) measured by two sensors is a function of time t as well as the coordinates x (machine direction) and y (cross direction).

The moving web with width $b = 41$ cm is supported by two pairs of rollers A and D that are set apart from each other by length $L = 88$ cm and two other supporting rollers B and C. The actuator consists of a simple loudspeaker which sends the sound waves to attenuate the transverse vibrations of the web. Table 1 shows the main mechanical parameters of two printing materials used for the tests.

It is assumed that the web is transferred in the x direction with an axially translatory speed V and is subjected to a uniform in-plane tension $T = 40$ N.

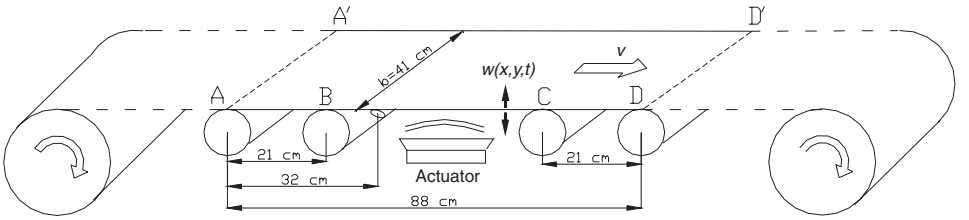

Fig. 1. Experimental setup configuration.

Table 1
Printing materials

Printing material	Thickness, h (mm)	Density, ρ (kg m^{-3})	Young modulus, E (N m$^{-2)}$	Poisson's coefficient, v
Self-adhesive paper	0.14	1214	8×10^9	0.3
Polyethylene PE plastic film	0.05	920	$0{\cdot}29 \times 10^9$	0.4

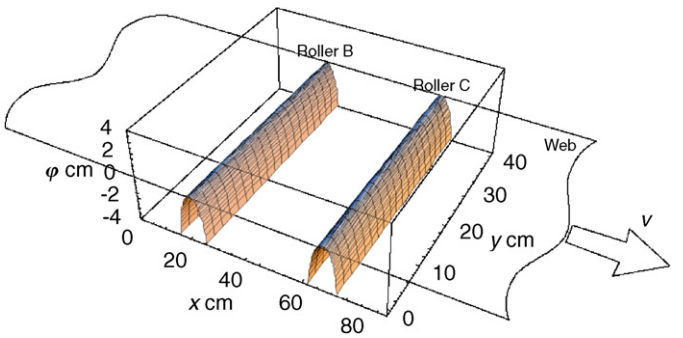

Fig. 2. Graph of φ.

3. Theoretical analysis

3.1. Nonlinear model of the flexible web

The mathematical model which characterizes the vertical out-of-plane displacement $w(x, y, t)$ of the web in zones A–D (Fig. 1), with obstacles B and C, is analyzed in this subsection.

The first step is to introduce the domain $\Omega = [0,L] \times [0, b]$ and a function φ whose graph (Fig. 2) represents the physical profile of the rollers in contact with the web. Thanks to this function, it becomes clear that rollers are obstacles for the web, with the condition $w \geqslant \varphi$.

The distributed parameter system represented in Fig. 1, assuming the translating speed $V = 0\,\mathrm{m\,s^{-1}}$, is described by the following two-dimensional partial differential equation [2,3]:

$$\rho h \frac{\partial^2 w}{\partial t^2} = \frac{T}{b}\frac{\partial^2 w}{\partial x^2} - D\left(\frac{\partial^4 w}{\partial x^4} + 2\frac{\partial^4 w}{\partial x^2 \partial y^2} + \frac{\partial^4 w}{\partial y^4}\right) + F, \quad (x, y) \in \Omega, t \geqslant 0, \tag{1}$$

where $w(x, y, t)$ is the vertical displacement of the web, $D = (1/12)Eh^3/(1-v^2)$ is the flexural rigidity and F is the force per unit area exerted by the roller on the flexible web. This force represents the nonlinear term in Eq. (1). The other parameters are explained in Table 1.

To well identify the problem, the boundary conditions must be specified. At the boundaries of the web (contact lines AA′ and DD′ in Fig. 1), $w(x, y, t)$ satisfies

$$w = 0, \quad \frac{\partial w}{\partial x} = 0, \quad x = 0, \quad x = L, \quad y \in [0, b], \quad t \geqslant 0. \tag{2}$$

The conditions at the lateral boundaries are expressed as follows:

$$\begin{aligned} &\frac{\partial^2 w}{\partial y^2} + v\frac{\partial^2 w}{\partial x^2} = 0, \\ &\frac{\partial^3 w}{\partial y^3} + (2 - v)\frac{\partial^3 w}{\partial x^2 \partial y} = 0, \\ &x \in [0, L], \quad y = 0, \quad y = b, t \geqslant 0. \end{aligned} \tag{3}$$

The condition for obstacles (rollers B and C in Fig. 1) can be expressed as

$$w \geqslant \varphi \quad (x, y) \in \Omega, \quad t \geqslant 0. \tag{4}$$

The initial conditions for Eq. (1) are specified as follows:

$$w = w_0, \quad \frac{\partial w}{\partial t} = w_1, \quad (x, y) \in \Omega, \quad t = 0, \tag{5}$$

where w_0 and w_1 are given functions.

In Eq. (1), $w(x, y, t)$ and F are unknown functions and the conditions given by Eqs. (2)–(5) do not allow them to be determined. To obtain the solution $w(x, y, t)$, the interaction between rollers B and C and the flexible web must be specified. The penalization approach [12] enables a nonlinear analysis of this interaction. From a mathematical point of view, this method leads to theoretical results as well as numerical schemes of resolution.

The principle of the penalization approach to mathematical problems with unilateral constraints consists in putting condition (4) in Eq. (1) by replacing F with a force F_ε of large intensity which acts on the flexible web at points where $w < \varphi$.

Setting

$$(x)_- = \begin{cases} x \text{ if } x < 0, \\ 0 \text{ if } x \geqslant 0, \end{cases}$$

the choice can be

$$F_\varepsilon = -\frac{1}{\varepsilon}(w - \varphi)_- \quad \text{or} \quad F_\varepsilon = \frac{1}{\varepsilon}(w - \varphi)_- \left(\frac{\partial w}{\partial t}\right)_-, \tag{6}$$

where ε is a small positive parameter.

The spring force in the first term in Eq. (6) gives the model for the elastic shock with energy conservation between rollers B and C and the web, the second one characterizes a soft shock with energy dissipation.

By solving Eq. (1) after the substitution with the conditions given by Eqs. (2), (3) and (5) gives a family of functions w_ε and making ε tend towards 0, one obtains a solution of Eq. (1) which satisfies Eq. (4). The solution of the penalty formulation is computed, using force $F_\varepsilon = (1/\varepsilon)(w - \varphi)_-(\partial w/\partial t)_-$ with the following initial conditions:

$$w_0 = 0 \quad \text{and} \quad w_1 = \begin{cases} 1 & \text{if} \quad 0.39 \leqslant x \leqslant 0.49 \quad \text{and} \quad 0.164 \leqslant y \leqslant 0.246, \\ 0 & \text{else} \end{cases} \tag{7}$$

with choice $\varepsilon = 5 \times 10^{-9}$. With these initial conditions, the partial differential equation describes the displacement of the web, initially at rest, which is excited by an impulse approximately located in the center of domain Ω. To solve this problem numerically, we use a finite difference method. We introduce a time step $\Delta t > 0$, meshes $\Delta x = L/M$ and $\Delta y = b/N$ where M and N are integers, points $(x_i, y_j) \in \Omega$ defined by $x_i = i\Delta x$, $y_j = j\Delta y$ with $0 \leqslant i \leqslant M$, $0 \leqslant j \leqslant N$ and times $t_K = K\Delta t$.

Using the discrete derivation formula [13], the differential problem is replaced by systems of algebraic equations whose solutions denoted by $w^K_{\varepsilon,ij}$ are approximations of $w_\varepsilon(x_i, y_j, t_K)$. The Mathematica software is used to compute this numerical solution which is shown in Fig. 3.

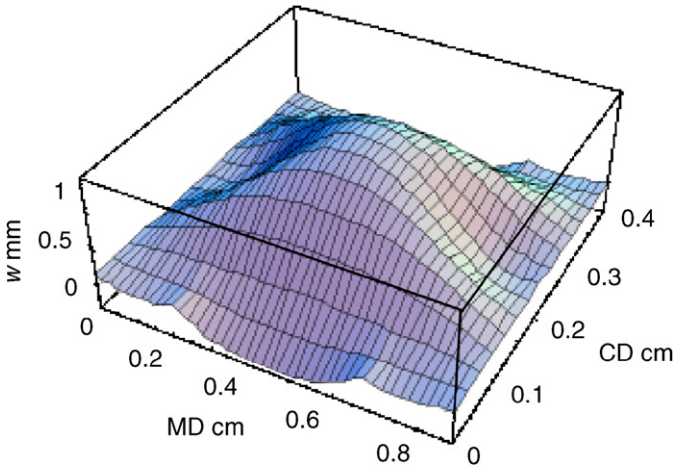

Fig. 3. Graph of w at time $t = 0.027$ s.

By applying the Fourier transform to function w_e, the frequency response at point $x = 44$ cm, $y = 20$ cm can be computed. This gives the following two frequencies of out-of-plane vibrations with the numerical values given in Table 1 for the case of self-adhesive paper:

$$f_1 = 16.72\,\text{Hz}, \quad f_2 = 37.15\,\text{Hz}. \tag{8}$$

3.2. Frequencies taking account of the surrounding airflow

The natural frequencies in the (i,j) mode, where i and j represent the orders of mode complexities in the x (MD) and y (CD) directions, can be obtained from the linear model formulas given in Ref. [1], as follows:

$$\begin{aligned} f_{11\_T} &= 15.22\,\text{Hz}, \\ f_{21\_T} &= 29.41\,\text{Hz}, \quad f_{31\_T} = 43.17\,\text{Hz}. \end{aligned} \tag{9}$$

The frequencies given by Eqs. (8) and (9) are calculated without taking account of the interaction between the web and surrounding air. These values are greater than the actual values obtained from experimental results on the test bed. If the mass of the surrounding fluid $\boldsymbol{M}_a$ is added to the mass of the flexible material $\boldsymbol{M}_p$, the eigenfrequencies are calculated [1,11] using

$$f_{ij\_\text{Air}} = \frac{f_{ij\_T}}{\sqrt{1 + \dfrac{M_a}{M_p}}}. \tag{10}$$

For the numerical values given in Table 1 for self-adhesive paper, M_p becomes

$$M_p = \rho h b L = 1214 \times 0.14 \times 10^{-3} \times 0.41 \times 0.88 = 0.0613\,\text{kg}. \tag{11}$$

The mass of surrounding air depending on the ratio L/b of the web, on the boundary conditions and on the vibration mode is given by expression [1]

$$M_a = \alpha \frac{\pi}{4} \rho_a b^2 L. \tag{12}$$

The coefficient α in Eq. (12) also depends on the aspect ratio of the web. For the experimental setup $\alpha = 0.7714$, the value of M_a is calculated as follows:

$$M_a = 0.7714 \times \frac{\pi}{4} \times 1.2 \times 0.41^2 \times 0.88 = 0.1075\,\text{kg}. \tag{13}$$

The first three frequencies calculated by incorporating the effect of surrounding air are then

$$f_{11\_Air} = 9.17\,\text{Hz},$$
$$f_{21\_Air} = 17.72\,\text{Hz}, \quad f_{31\_Air} = 26.02\,\text{Hz}. \tag{14}$$

By taking account of the mass of surrounding air for the two frequencies calculated in Eq. (8), the following values are obtained:

$$f_1 = 10.06\,\text{Hz}, \quad f_2 = 22.88\,\text{Hz}. \tag{15}$$

Such a model enables the dynamic analysis of the printing web with various material properties and parameters.

The comparison of the fundamental frequency computed with a linear and a nonlinear model (Eqs. (14) and (15)) shows that the linear theory underestimates this frequency. Discrepancies in the frequencies calculated by Eqs. (14) and (15) can be attributed to the obstacles (Rollers B and C in Fig. 1) present in the nonlinear model.

Note that the translatory speed, in this section, is assumed to be 0. If this speed is nonzero, the natural frequencies decrease when the speed increases as shown by the following equation:

$$f_n = \frac{nc_0}{2L}\sqrt{1-\left(\frac{V}{c_0}\right)^2}, \quad n = 1,2,3\ldots. \tag{16}$$

Kim et al. [14] investigated the divergence instability regions that occur in the neighborhood of the critical speed given by

$$c_0 = \sqrt{\frac{T}{\rho hb + m_a}}, \tag{17}$$

where the mass of surrounding air per unit length of the web m_a (kg m^{-1}) is deduced from Eq. (13) taking account of the obstacles represented by rollers B and C in Fig. 1.

Pellicano [15] showed that the dynamics of axially moving webs is greatly affected by the transportation speed, especially beyond a critical value which depends on the flexural stiffness and the applied tension. It is to be noticed that the value of the critical speed for self-adhesive paper $c_0 = 16.66\,\text{m s}^{-1}$ lies far above the translatory speed used in this experimental setup.

These theoretical results will be compared with the experimental ones described in the next section.

4. Experimental analysis

4.1. Excitation by the cam

In this subsection, the experimental results of vertical web displacement in the case of excitation at a frequency near the 1st vibration mode ($f = 13.2\,\text{Hz}$) by a cam are presented in the time and frequency domain. The cam is located at $x = 32\,\text{cm}$ related to point A in Fig. 1. To obtain the 3D and 2D profiles, 14 times 9 sensor locations were chosen as shown in Table 2.

For self-adhesive paper, the amplitudes of vibration spectra measured at each of the 126 points are plotted for the 1st and 2nd vibration modes in Figs. 4 and 5, respectively. The standard deviation (SD) of the time signals measured at the same sensor locations are presented in Figs. 6 and 7.

Standard deviation is used because it characterizes the energy of the vibrations and is measured with the same units as the original data.

Table 2
Displacement sensors locations

x-Axis (cm)	11	13	29	30	31	32	34	42	48	56	59	75	78
y-Axis (cm)	1	5	10	15	21	26	31	36	40				

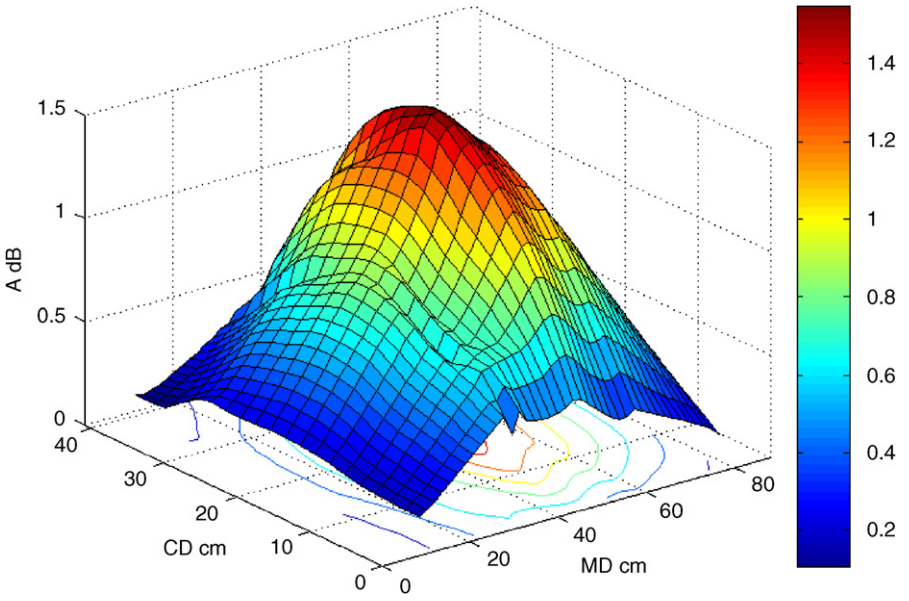

Fig. 4. 3D profile of the main vibration mode (13.2 Hz) in the frequency domain.

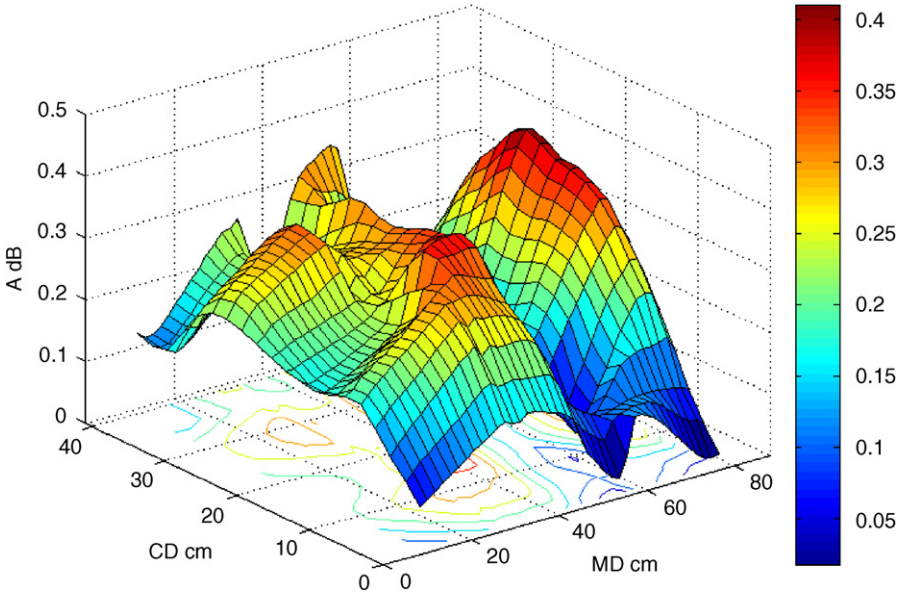

Fig. 5. 3D profile of the second vibration mode (26.4 Hz) in the frequency domain.

According to the central limit theorem, if there are several variables causing the web vibrations, these can be characterized by Gaussian distribution which is described by the mean value and by SD.

The comparison of the 3D profiles in the time domain (Fig. 6) with the 1st vibration mode in the frequency domain (Fig. 4) confirms that the time history characterizes the main vibration mode of the flexible web.

This mode has a maximum in the center of the web with an amplitude gradually diminishing towards the 4 edges. For the 2nd vibration mode (Fig. 5), a maximum can be observed near the location at $x = 70$ cm and a minimum at $x = 60$ cm. For the accurate observation of the 2nd vibration mode, the feedback sensor should be located in the central position of the flexible web with the local maximum (see Fig. 5). The proposed location for the sensor for the 1st mode should also be in the central zone of the range from $x = 40$–60 cm, as shown in Fig. 7.

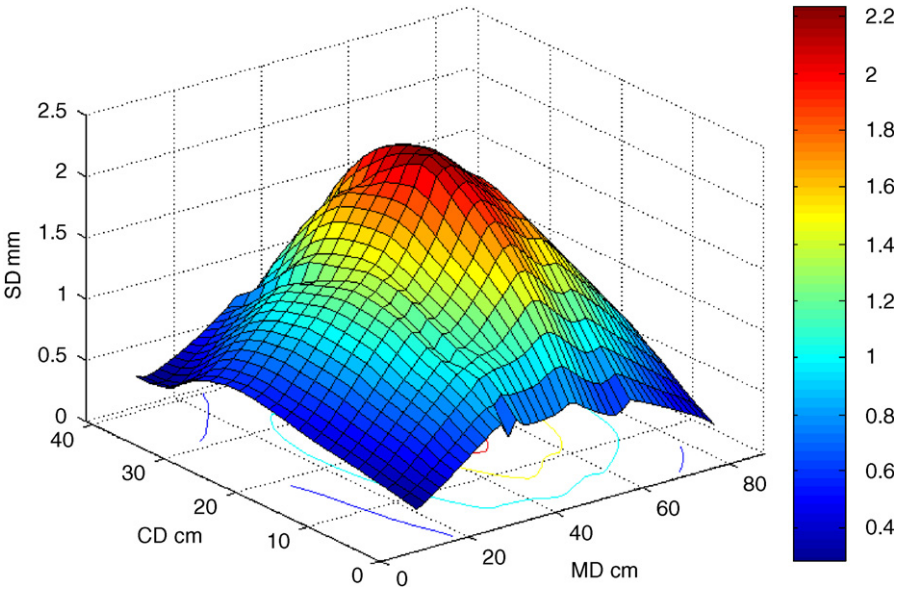

Fig. 6. 3D profile of the standard deviation of the vibration amplitude.

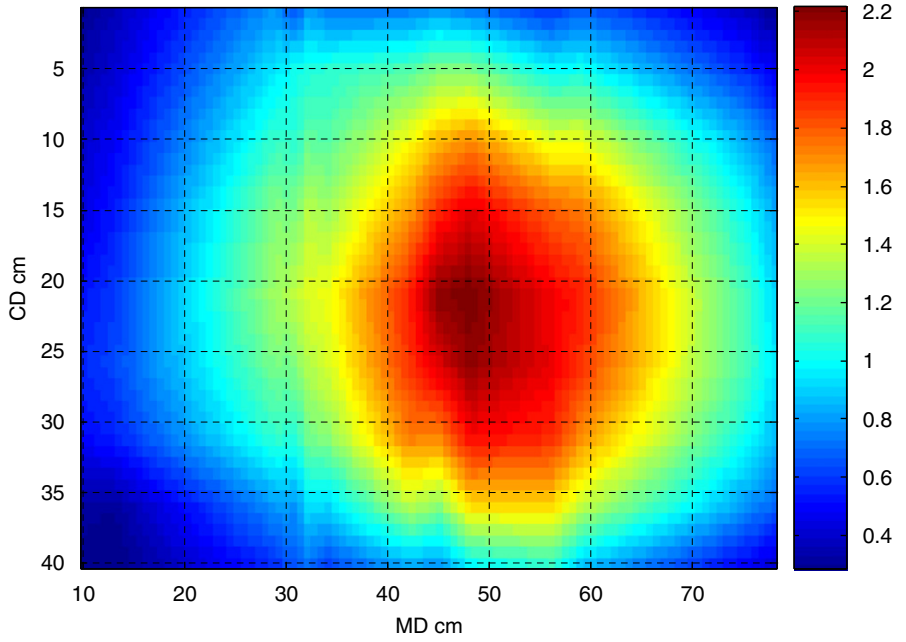

Fig. 7. 2D profile of the standard deviation of the vibration amplitude.

The experimental results obtained for the PE are similar and are not presented in this section.

4.2. *Excitation by a loudspeaker*

The experimental identification is based on the analysis of measurements of the flexible web displacement due to excitation signal fed to the loudspeaker.

The control signal is a multisine sum of 512 harmonic signals in the range 0–125 Hz of the same amplitude and with a random harmonic phase. The main properties of this type of signal for identification in the

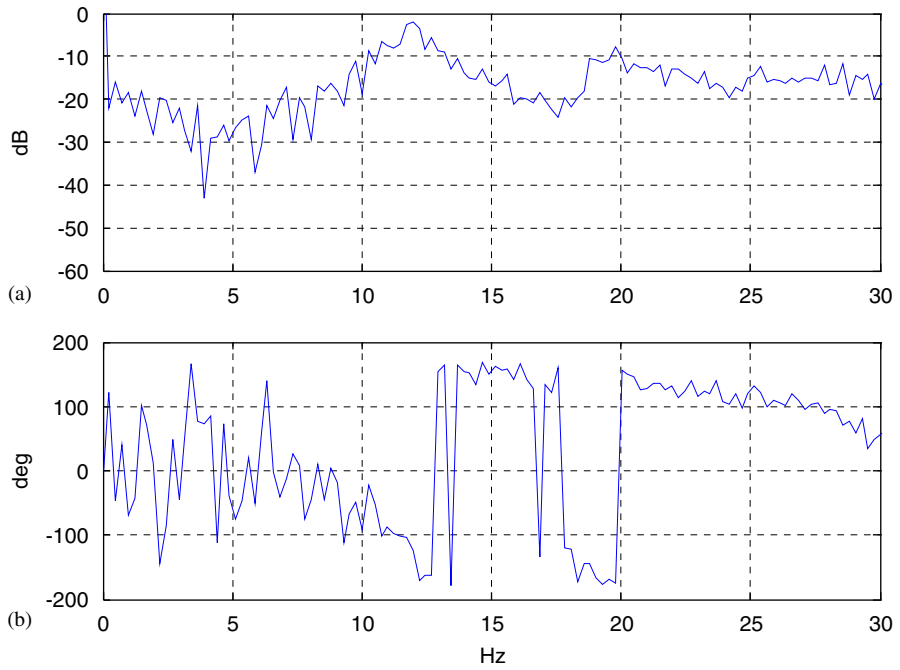

Fig. 8. Frequency responses of self-adhesive paper with tension $T = 40$ N: (a) amplitude response and (b) phase response.

frequency domain are described in Ref. [16]. An extensive comparative study of exciting signals is carried out in Ref. [17].

The data obtained with multisine signals are used to estimate the frequency response function (Fig. 8) as the ratio of the mean values of the Fourier coefficients at the discrete test frequencies.

From this frequency response, the mode shapes, natural frequencies and damping ratios [18] can be obtained. The difference between the calculated main resonant frequency in Section 3.1 and the one measured in Fig. 8 (first resonance peak at $f_1 = 12$ Hz) is less than 20%. The reason for this discrepancy could be due to the fact that the theoretical model does not take account of the variation of tension in time and the fact that the flexible web slides on the cylinders. From the frequency responses measured at 9×14 points defined in Section 4.1, the 3D profile of the 1st vertical displacement mode thus excited by the loudspeaker shown in Fig. 9, is generated.

4.3. Conclusion

The results of the frequencies and mode shapes obtained with the two excitation techniques are quite similar. This highly justifies the use of a loudspeaker to generate the compensation signal.

The next section shows how to design a controller with an actuator and two displacement sensors so as to cancel out the first two vibration modes of the flexible web on the printing machine.

5. Controller design

The aim of this section is to design a digital controller to damp the two main vibration modes of the web. The objective is to design a control law for the actuator output $U(s)$ based on the measured information at the sensor locations x_1 and x_2 such that the web waves are cancelled out and the system is stabilized.

The controller was designed, using the process model characterized by the 1st and 2nd vibration modes.

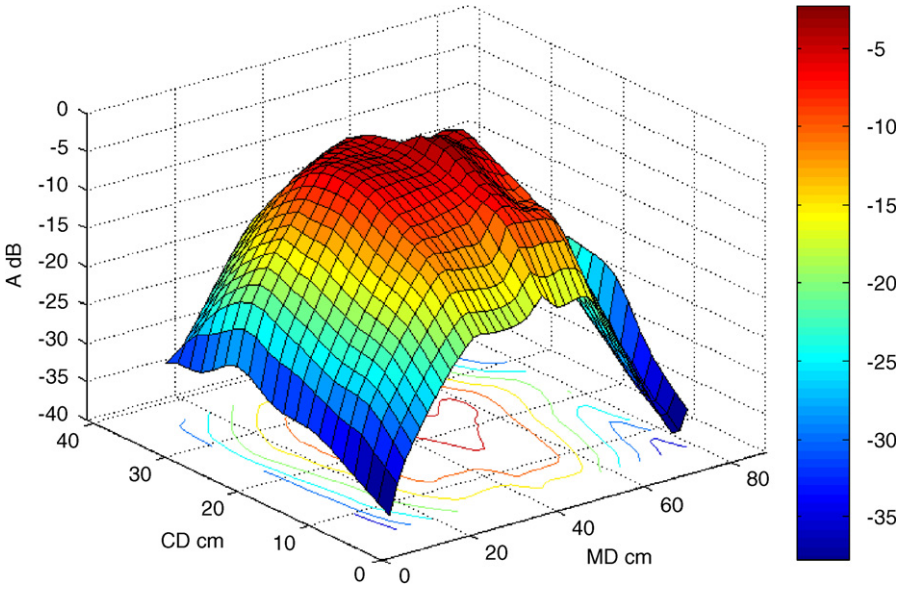

Fig. 9. 3D profile of the main vibration mode 12 Hz in the frequency domain.

As shown in Chung et al. [5] and Wang et al. [7], the control force expressed in the Laplace transform domain is given by

$$U(s) = \frac{-2s\left[H(x_1,s) - H(x_2,s)\mathrm{e}^{-\lambda_1\left(\frac{x_2-x_1}{c_0}\right)}\right]\mathrm{e}^{\lambda_2\left(\frac{x_a-x_1}{c_0}\right)}}{1-\mathrm{e}^{(\lambda_2-\lambda_1)\left(\frac{x_2-x_1}{c_0}\right)}}, \tag{18}$$

where $H(x_1, s)$ and $H(x_2, s)$ are Laplace transforms of the out-of-plane web displacements measured with sensors located at x_1 and x_2, an actuator located at x_a and

$$\lambda_1 = \frac{s}{1-\upsilon}, \quad \lambda_2 = \frac{-s}{1-\upsilon}. \tag{19}$$

In Eq. (19), $\upsilon = V/c_0$ is the dimensionless translatory speed and c_0 the wave propagation or critical speed given by Eq. (17). The numerical values of T, ρ, b, h in Section 2, lead to $c_0 = 16.66\,\mathrm{m\,s^{-1}}$.

For $V = 0\,\mathrm{m\,s^{-1}}$, the substitution of the approximation $e^{-\tau s} \cong (1-\frac{\tau}{2}s)/(1+\frac{\tau}{2}s)$ in Eq. (18) gives for the controller transfer function $R_1(s) = U_1(s)/H_1(s)$ and $R_2(s) = U_2(s)/H_2(s)$ the expressions:

$$R_1(s) = \underbrace{-\frac{1}{2\tau_1}\frac{-2\tau_2\tau_1 s^2 + (2\tau_1 - \tau_2)s + 1}{\tau_2 s + 1}}_{G_{c1}(s)} \underbrace{\frac{1}{\frac{s^2}{\omega_2^2} + 2\frac{\zeta s}{\omega_2} + 1}}_{G_2(s)} K_{p1}, \tag{20}$$

$$R_2(s) = \underbrace{\frac{1}{2\tau_1}\frac{-2\tau_1(\tau_1+\tau_2)s^2 + (\tau_1-\tau_2)s + 1}{(\tau_1+\tau_2)s + 1}}_{G_{c2}(s)} \underbrace{\frac{1}{\frac{s^2}{\omega_1^2} + 2\frac{\zeta s}{\omega_1} + 1}}_{G_1(s)} K_{p2}, \tag{21}$$

where

$$\tau_1 = \frac{(x_2 - x_1)}{2c_0} \quad \text{and} \quad \tau_2 = \frac{(x_a - x_1)}{2c_0}, \tag{22}$$

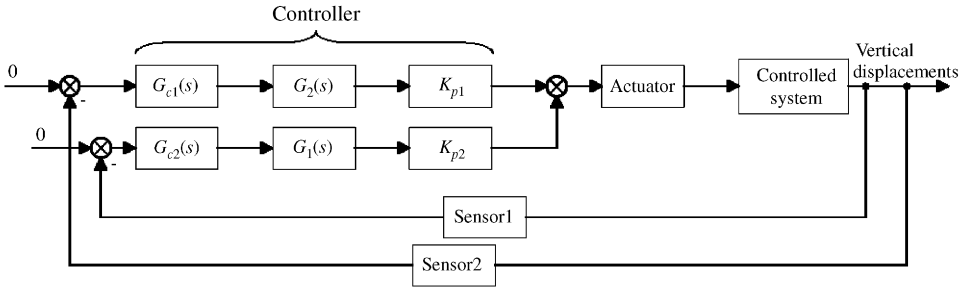

Fig. 10. Proposed structure for the active control of web vibrations.

ω_1 and ω_2 are the 1st and 2nd web vibration modes, respectively, with the damping factor ζ and K_{p1} and K_{p2} are the controller adjustable gains.

The optimal sensor locations are chosen at the positions where the corresponding vibrating modes have a maximum value (see Figs. 4 and 5).

Numerically, for the values $V = 0\,\mathrm{m\,s^{-1}}$, $x_1 = 45\,\mathrm{cm}$, $x_2 = 57\,\mathrm{cm}$ and $x_a = 50\,\mathrm{cm}$, the results are $\tau_1 = 0.0036\,\mathrm{s}$ and $\tau_2 = 0.0015\,\mathrm{s}$. Fig. 10 summarizes the structure of the proposed active vibration controller described in this section. Unlike the structure proposed in Refs. [5,7] in Eqs. (20) and (21), the controllers $G_{c1}(s)$ and $G_{c2}(s)$ (Fig. 10) are fitted with frequency selective filters $G_1(s)$ and $G_2(s)$ adjusted to $\omega_1 = 75.5\,\mathrm{rad\,s^{-1}}$ and $\omega_2 = 151\,\mathrm{rad\,s^{-1}}$ of the 1st and 2nd vibration modes respectively, with a damping factor $\zeta = 0.1$. Controller $R_1(s)$ using the signal from sensor 1 located at $x_1 = 45\,\mathrm{cm}$ compensates for the 2nd vibration mode, while controller $R_2(s)$ connected to the sensor 2 at $x_2 = 57\,\mathrm{cm}$ allows energy dissipation of the 1st mode. The other vibration modes are neglected. The parameters K_{p1} and K_{p2} in Eq. (20) and (20) are adjusted experimentally until an optimum is reached, taking account of the loudspeaker power electronics saturation at 12 V.

A discrete version of Eqs. (20) and (21) is implemented on a DSP with a sampling rate of 2 kHz. The results of the measurements on the test bed presented in the next section show a significant reduction in the amplitude of the out-of-plane vibrations of the flexible web, especially for the 1st and 2nd modes.

6. Experimental results

A number of experimental results will now be presented for two types of printing materials. The actuator and sensors are placed at the points defined by the analysis in Section 4.1.

In order to quantify the effect of the controller evaluated by the vertical displacement measured by Sensors 1 and 2 located at $x_1 = 45\,\mathrm{cm}$ and $x_2 = 57\,\mathrm{cm}$, respectively, the standard deviation (SD) of vibration levels is first calculated from the time histories.

The vibration spectra in the frequency domain, with and without control, are then compared. The tests are carried out with an excitation frequency of 12 Hz. For this frequency, found experimentally, the amplitude of the vertical displacement of the web is maximum for the above-defined sensor locations. The first two vibration modes are considered here.

The time response in Fig. 11(a), with the controller set at $t = 1.5\,\mathrm{s}$ for self-adhesive paper, is plotted for optimal values of controller gains K_{p1} and K_{p2} found from trial runs. Table 2 summarizes the results for time histories for three couples of gains K_{p1} and K_{p2}. It can be seen from Fig. 11(a) and Table 3 that the value of SD is divided by 3.31, going from 1.82 to 0.55 mm. The experimental frequency responses are shown in Fig. 11(b) without control and Fig. 11(c) with the controller. From Fig. 11, it is clear that the control scheme has a satisfactory vibration control effect, since the two main frequency peaks are eliminated, compared with the noncontrolled frequency response presented in Fig. 11(b). The results in the frequency domain are shown in Table 4, where the amplitude reduction of the 1st and 2nd vibration modes is evaluated with $F_{\text{reduction}} = A_{\text{without control}}/A_{\text{with control}}$. The fundamental peak is divided by about 5.7 and the 2nd mode peak by 7 with the proposed control. Similar results are obtained for the PE and are presented in Fig. 12 and in

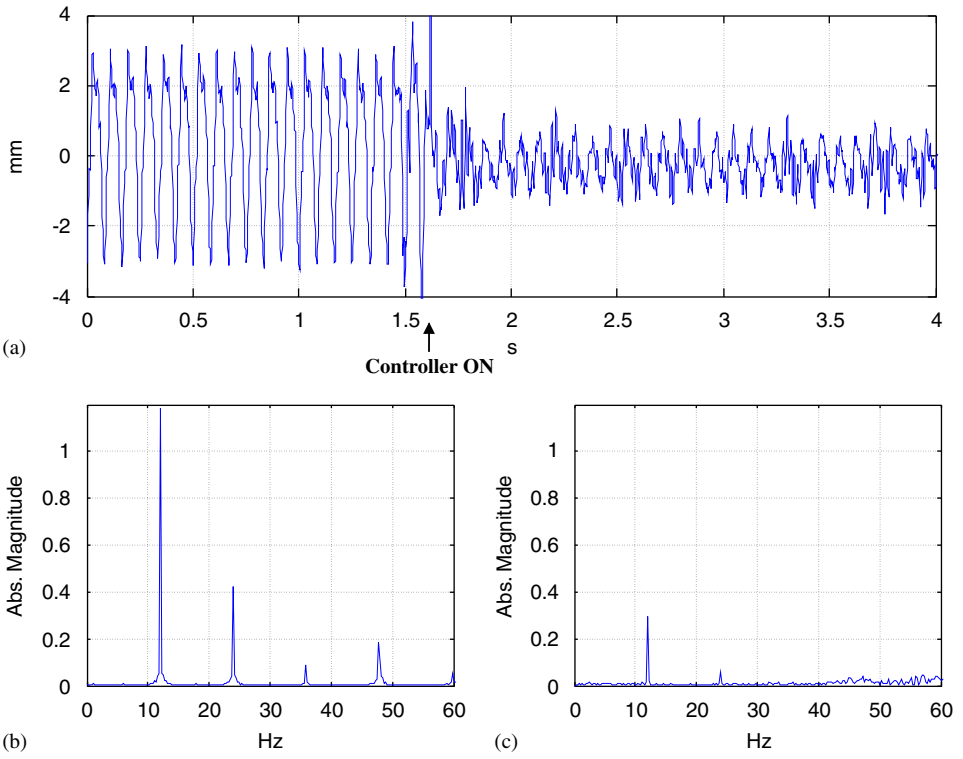

Fig. 11. Comparison of the experimental responses at $x_1 = 45$ cm (sensor 1) of self-adhesive paper without and with control ($K_{p1} = 7$ and $K_{p2} = 14$): (a) time response, (b) frequency response without control, and (c) frequency response with control.

Table 3
Comparison of standard deviation of vibration time history with and without control in the case of self-adhesive paper

Gain K_{p1}, K_{p2}	Sensor 1		Sensor 2		Loudspeaker control signal
	Standard deviation, SD_1 (mm)	$F_{reduction}$	Standard deviation, (SD_2) mm	$F_{reduction}$	Standard deviation, SD_a (V)
5, 10	0.65	2.80	0.61	3.49	2.48
6, 12	0.58	3.14	0.57	3.74	2.76
7, 14	0.55	3.31	0.57	3.74	3.08
Without control	1.82	—	2.13	—	—

_Toc109631062_Ref119808907_Toc121104645Table 4
Comparison of the amplitudes A of vibration spectra with and without control in the case of self-adhesive paper_Toc109631062_Ref119808907_Toc121104645

Gain K_{p1}, K_{p2}	Sensor 1				Sensor 2			
	First vibration mode		Second vibration mode		First vibration mode		Second vibration mode	
	A (mm)	$F_{reduction}$	A (mm)	$F_{reduction}$	A (mm)	$F_{reduction}$	A (mm)	$F_{reduction}$
5, 10	0.40	2.95	0.09	4.67	0.36	4.11	0.15	1.07
6, 12	0.36	3.28	0.08	5.25	0.29	5.10	0.16	1.00
7, 14	0.30	3.93	0.06	7.00	0.26	5.69	0.15	1.07
Without control	1.18	—	0.42	—	1.48	—	0.16	—

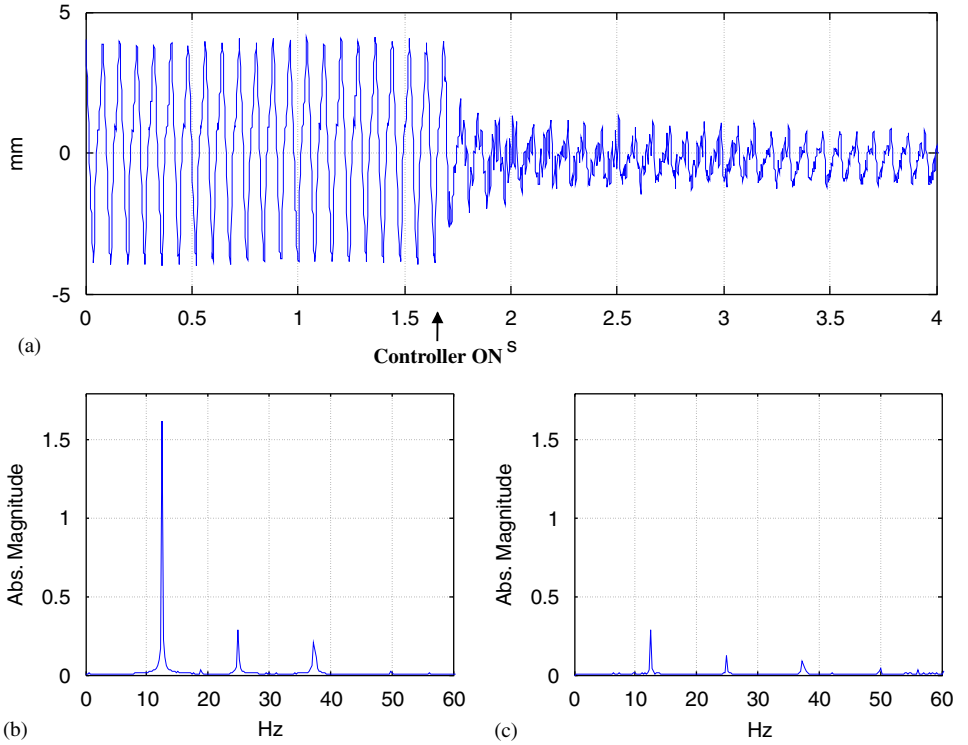

Fig. 12. Comparison of the experimental responses at $x_1 = 45$ cm (sensor 1) of polyethylene with and without control ($K_{p1} = 4$ and $K_{p2} = 10$): (a) time response, (b) frequency response without control, and (c) frequency response with control.

Table 5
Comparison of standard deviation of vibration time history with and without control in the case of polyethylene (PE) plastic film

Gain K_{p1}, K_{p2}	Measurement point: sensor 1		Measurement point: sensor 2		Loudspeaker control signal
	Standard deviation, SD_1 (mm)	$F_{reduction}$	Standard deviation, SD_2 (mm)	$F_{reduction}$	Standard deviation, SD_a (V)
3, 6	0.73	3.32	0.69	3.10	1.63
4, 8	0.60	4.03	0.57	3.75	1.83
4, 10	0.56	**4.32**	0.57	**3.75**	2.11
Without control	2.42	—	2.14	—	—

Tables 5 and 6. From these tables, it can be concluded that, in the time domain, the controller reduces vibrations, dividing them by 4.32 and 3.75 for Sensors 1 and 2, respectively.

In the frequency domain, the controller reduces the frequency peak amplitude from 0.29 to 0.13 mm for Mode 2 measured by Sensor 1. The 1st mode measured by this sensor is reduced from 1.62 to 0.29 mm. For the 1st mode and Sensor 2, the controller reduces the frequency peak amplitude of the PE to 0.3 mm.

The last column in Tables 3 and 5 characterizes the control signal applied to the loudspeaker amplifier. Note that the best performance obtained for the controller gains $K_{p1} = 7$, $K_{p2} = 14$ (Table 3) and $K_{p1} = 4$, $K_{p2} = 10$ (Table 5) for self-adhesive paper and PE, respectively, do not correspond as expected to the minimum control stress. The controller design method based on the minimization of the integral control energy together with the kinetic and potential energy of the flexible web is presented in Ref. [5].

In practical applications, the controller must be robust with respect to parametric uncertainties, such as errors expected in frequencies ω_1 and ω_2 or in the damping factor ζ in Eqs. (20) and (21). The robustness of the

Table 6
Comparison of the amplitudes of vibration spectra with and without control in the case of polyethylene (PE) plastic film

Gain K_{p1}, K_{p2}	Measurement by sensor 1				Measurement by sensor 2			
	First vibration mode		Second vibration mode		First vibration mode		Second vibration mode	
	A (mm)	$F_{reduction}$	A (mm)	$F_{reduction}$	A (mm)	$F_{reduction}$	A (mm)	$F_{reduction}$
3, 6	0.46	3.50	0.15	1.93	0.44	3.30	0.10	1.3
4, 8	0.36	4.47	0.14	2.07	0.35	4.14	0.11	1.18
4, 10	**0.29**	5.55	0.13	2.23	0.30	4.83	0.10	1.3
Without control	**1.62**	—	0.29	—	1.45	—	0.13	—

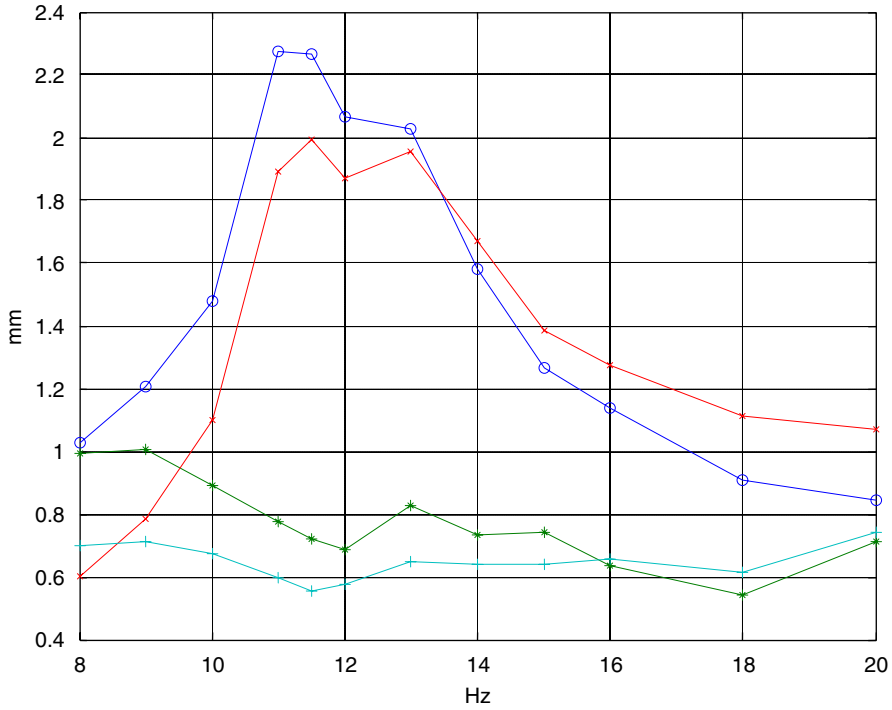

Fig. 13. Standard deviation in mm at sensors 1 and 2 vs. excitation frequency for self-adhesive paper with and without control ($K_{p1} = 6$, $Kp_2 = 12$). o: SD_1 without compensation; *: SD_1 with compensation; x: SD_2 without compensation; +: SD_2 with compensation.

controller is verified by changing the excitation frequency in the range 8–20 and 10–18 Hz for self-adhesive paper and PE, respectively. Figs. 13 and 14 compare the standard deviation of the time history with and without active vibration compensation for different values of the excitation frequency. It appears that with a 50% modelling error, the controller is still effective.

The robustness of the proposed control scheme with respect to other parameter variations, such as in-plane tension applied to the web, is also confirmed in the experimental setup.

7. Conclusion

This paper has presented an analytical and experimental modelling process for the vertical vibrations of a flexible web of a printing machine. Active compensation for vibrations, using two sensors, an actuator without contact with the moving web and two controllers, was implemented on a DSP and experimentally verified on a

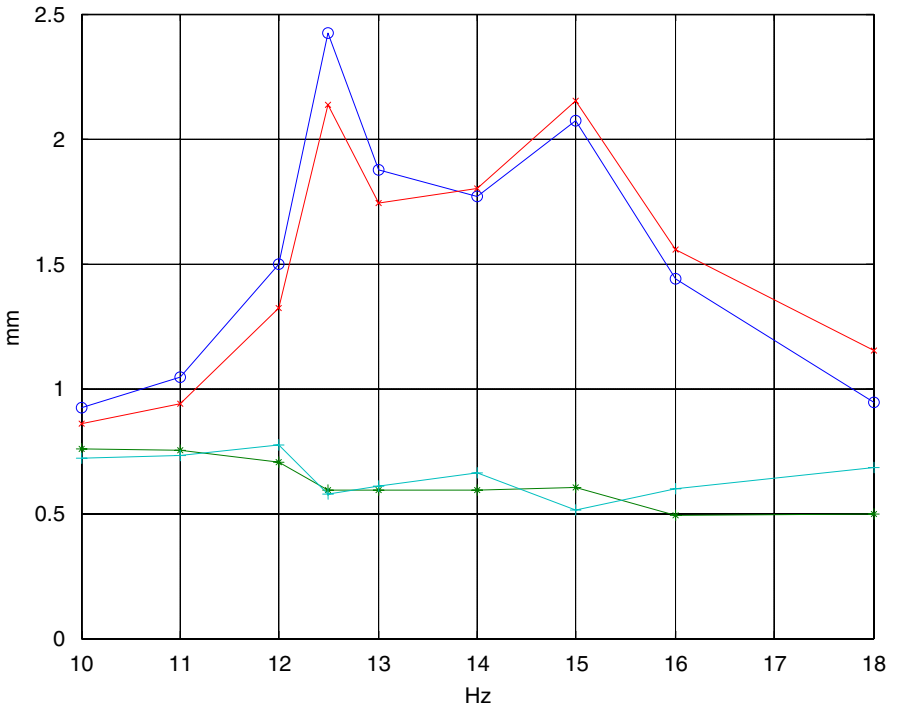

Fig. 14. Standard deviation in mm at sensors 1 and 2 vs. excitation frequency for plastic film (PE) with and without control ($K_{p1} = 4$, $K_{p2} = 8$). o: SD_1 without compensation; *: SD_1 with compensation; *x*: SD_2 without compensation; +: SD_2 with compensation.

test bed. The amplitudes of the 1st and 2nd vibration modes were significantly reduced and the robustness related to the variation of parameters verified.

For future research issues, the consideration of the machine speed variation and other types of sensors, such as acceleration sensors, need to be investigated. Further development will involve reliability and maintainability tests for the components, such as loudspeakers, in the printing machine environment.

Acknowledgments

This work was supported by the Research fund of the University of Applied Sciences of West Switzerland (Project No. HES-SO:AI-05-02).

The authors are grateful to Dr. Friedhelm Altpeter from Charmilles Technologies SA in Geneva for the highly interesting discussions and helpful suggestions.

References

[1] R.D. Blevins, *Formulas for Natural Frequency and Mode Shape*, Robert E. Krieger Publishing Company, Malabar, 1979.
[2] L. Meirovich, *Analytical Methods in Vibrations*, Macmillan, New York, 1967.
[3] S.P. Timoshenko, *Théorie de la stabilité élastique*, Dunod, Paris, 1966.
[4] Ch.D. Rahn, *Mechatronic Control of Distributed Noise and Vibrations*, Springer, Berlin, 2001.
[5] C.H. Chung, C.A. Tan, Active vibration control of the axially moving string by wave cancellation, *Journal of Vibration and Acoustics* 117 (1995) 49–55.
[6] H.-K. Lee, S.-T. Chen, A.-C. Lee, Optimal control of vibration suppression in flexible systems via dislocated sensor/actuator positioning, *Journal of The Franklin Institute* 333 (B) (1996) 789–802.
[7] J. Wang, Q. Li, Active vibration control methods of axially moving materials—A review, *Journal of Vibration and Control* 10 (2004) 475–491.
[8] I.N. Kar, T. Miyakura, K. Seto, Bending and torsional vibration control of a flexible plate structure using H_∞-based robust control law, *IEEE Transactions on Control Systems Technology* 8 (2000) 545–553.

[9] K. Matsuda, Y. Okada, Sensorless active suppression of transverse vibration of flexible plate DE-ASME, *Design Engineering Technical Conference* 84 (3) (1995) 589–594.
[10] J. Yuan, Robust vibration control based on identified model, *Journal of Sound and Vibration* 269 (2004) 3–17.
[11] A. Pramila, Sheet flutter and interaction between sheet and air, *Tappi Journal* (1986) 70–74.
[12] A. Bamberger, M. Schatzman, New results on the vibrating string with a continuous obstacle, *SIAM Journal on Mathematical Analysis* 14 (1983) 560–595.
[13] W.T. Thomson, *Theory of Vibration with Applications*, Prentice-Hall, Inc, Englewood Cliffs, NJ, 1981.
[14] J. Kim, J. Cho, U. Lee, S. Park, Modal spectral element formulation for axially moving plates subjected to in-plane axial tension, *Computers & Structures* 81 (2003) 2011–2020.
[15] F. Pellicano, On the dynamic properties of axially moving systems. *Journal of Sound and Vibration*. Online appendix, JSV 2005 〈http://www.elsevier.com/locate/jsvi〉.
[16] K.R. Godfrey, A.H. Tan, H.A. Barker, B. Chong, A survey of readily accessible perturbation signals for system identification in frequency domain. *Control Engineering Practice*, Online appendix, 2005 〈http://www.elsevier.com/locate/conengprac〉.
[17] C. Evans, P.J. Fleming, D.C. Hill, J.P. Norton, I. Pratt, D. Rees, K. Rodriguez-Vazquez, Application of system identification techniques to aircraft gas turbine engines, *Control Engineering Practice* 9 (2001) 135–148.
[18] D. Inman, *Engineering Vibration*, Prentice-Hall Inc, Englewood Cliffs, NJ, 1996.